BIOCHEMISTRY

 Volume 45, Number 17 May 2, 2006

Accelerated Publications

A Coupled Dinuclear Iron Cluster that Is Perturbed by Substrate Binding in *myo*-Inositol Oxygenase†

Gang Xing,‡ Lee M. Hoffart,‡ Yinghui Diao,‡ K. Sandeep Prabhu,§ Ryan J. Arner,§ C. Channa Reddy,§ Carsten Krebs,*,‡,|| and J. Martin Bollinger, Jr.*,‡,||

Departments of Biochemistry and Molecular Biology, Veterinary and Biomedical Sciences, and Chemistry, The Pennsylvania State University, University Park, Pennsylvania 16802

Received September 27, 2005; Revised Manuscript Received February 17, 2006

ABSTRACT: *myo*-Inositol oxygenase (MIOX) uses iron as its cofactor and dioxygen as its cosubstrate to effect the unique, ring-cleaving, four-electron oxidation of its cyclohexan-(*1,2,3,4,5,6-hexa*)-ol substrate to D-glucuronate. The nature of the iron cofactor and its interaction with the substrate, *myo*-inositol (MI), have been probed by electron paramagnetic resonance (EPR) and Mössbauer spectroscopies. The data demonstrate the formation of an antiferromagnetically coupled, high-spin diiron(III/III) cluster upon treatment of solutions of Fe(II) and MIOX with excess O_2 or H_2O_2 and the formation of an antiferromagnetically coupled, valence-localized, high-spin diiron(II/III) cluster upon treatment with either limiting O_2 or excess O_2 in the presence of a mild reductant (e.g., ascorbate). Marked changes to the spectra of both redox forms upon addition of MI and analogy to changes induced by binding of phosphate to the diiron(II/III) cluster of the protein phosphatase, uteroferrin, suggest that MI coordinates directly to the diiron cluster, most likely in a bridging mode. The addition of MIOX to the growing family of non-heme diiron oxygenases expands the catalytic range of the family beyond the two-electron oxidation (hydroxylation and dehydrogenation) reactions catalyzed by its more extensively studied members such as methane monooxygenase and stearoyl acyl carrier protein Δ^9-desaturase.

myo-Inositol oxygenase (MIOX,[1] EC 1.13.99.1) catalyzes production of D-glucuronate (DG) from *myo*-inositol (MI) and dioxygen (Scheme 1) (*1*−*3*). This glycol-cleaving, four-electron-oxidation reaction is the first step in the only known pathway in humans for catabolism of MI (*4*), the sugar backbone of the important signaling molecules known collectively as phosphoinositides. It has been suggested that depletion of MI caused by altered levels of MIOX expression or activity (or both) may contribute to the myriad complications commonly associated with diabetes mellitus (e.g., neuropathy, nephropathy, retinopathy, and cataracts) and,

† This work was supported by an Innovative Biotechnology Seed Grant from Johnson and Johnson and The Huck Institutes of the Life Sciences at The Pennsylvania State University.

* To whom correspondence should be addressed. J.M.B.: Department of Biochemistry and Molecular Biology, 208 Althouse Laboratory, University Park, PA 16802; phone, (814) 863-5707; fax, (814) 863-7024; e-mail, jmb21@psu.edu. C.K.: Department of Biochemistry and Molecular Biology, 306 South Frear Building, University Park, PA 16802; phone, (814) 865-6089; fax, (814) 863-7024; e-mail, ckrebs@psu.edu.

‡ Department of Biochemistry and Molecular Biology.

§ Department of Veterinary and Biomedical Sciences.

|| Department of Chemistry.

[1] Abbreviations: MIOX, *myo*-inositol oxygenase; DG, D-glucuronate; MI, *myo*-inositol; AF, antiferromagnetic(ally); δ, Mössbauer isomer shift; ΔE_Q, Mössbauer quadrupole splitting parameter; Uf, uteroferrin; sMMO, soluble methane monooxygenase.

10.1021/bi0519607 CCC: $33.50
Published on Web 04/08/2006

Scheme 1: Reaction Catalyzed by *myo*-Inositol Oxygenase (MIOX)[a]

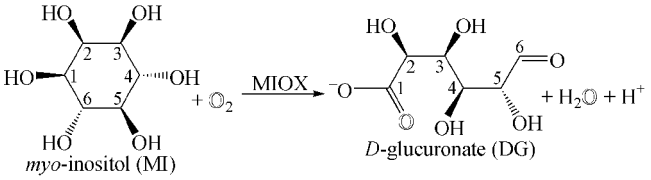

[a] The O atoms derived from dioxygen are shown in shadow font (*3*).

therefore, that MIOX could be a target for drugs to combat diabetic complications (*5*−*10*). An understanding of its structure and mechanism would facilitate design of potentially therapeutic MIOX inhibitors.

MIOX was first described and shown to require iron nearly five decades ago (*1*, *2*), but little insight into the nature of its iron cofactor or its catalytic mechanism has subsequently been reported. Recently, the gene encoding MIOX from pig kidney was isolated (*11*), and MIOXs from several sources (including mouse kidney, the original source of the recombinant enzyme studied in this work) were expressed in *Escherichia coli* (*12*). These achievements alleviated the scarcity of the enzyme that was at least partly responsible for the slow progress and set the stage for this study, in which we have defined the nature of the iron cofactor and examined its interaction with MI by spectroscopic methods. The data reveal that recombinant mouse MIOX can harbor a coupled dinuclear iron cluster, which, in its II/III and III/III oxidation states, is significantly perturbed by binding of MI in a manner that could be explained by direct coordination of the substrate, possibly in a bridging mode. As data in the accompanying paper (*13*) indicate that substrate-free mixed-valent MIOX is stable for many hours in the presence of O_2 but the substrate complex reacts rapidly with O_2 to generate DG, we suggest that coordination of MI simultaneously conditions the cluster for activation of O_2 to a species that can attack the substrate and activates the substrate for this attack.

MATERIALS AND METHODS

Materials. Growth medium components and biochemical reagents used in overexpression and purification of MIOX were obtained from sources listed previously (*14*). ^{57}Fe metal from Advanced Materials and Technologies, Inc. (New York, NY), was dissolved in 1 M H_2SO_4 ($H^+/Fe^0 = 4$) to convert it to ^{57}Fe(II). *myo*-Inositol was obtained from Sigma (St. Louis, MO).

Preparation of Apo MIOX. The previously described BL21(DE3) *E. coli* strain engineered to overexpress *Mus musculus* kidney MIOX (*12*) was grown at 37 °C with vigorous shaking in enriched medium [35 g/L tryptone, 20 g/L yeast extract, and 5 g/L NaCl (pH 7.3)] supplemented with 150 mg/L ampicillin until cultures reached an optical density at 600 nm of 0.6−0.9. 1,10-Phenanthroline dissolved in 0.1 N HCl was then added to the cultures to a final concentration of 0.5 mM. Treatment with this cell-permeative chelator prevents uptake of iron by MIOX during expression and purification (*15*). After a 15 min incubation to allow for iron chelation, overexpression of MIOX was induced by the addition of IPTG to a final concentration of 1 mM and *myo*-inositol to 40 mM. The cultures were shaken at 37 °C for an additional 3 h. The cells were harvested at 4 °C by centrifugation at 8000*g* for 15 min. The cells were then washed with a Tris-buffered saline solution [25 mM Tris, 140 mM NaCl, and 5 mM KCl (pH 7.4)] by resuspension and centrifugation. A yield of 3.5−4 g of wet cell mass per liter of culture was typical. The harvested cells were frozen in liquid nitrogen and stored at −80 °C until they were used.

All steps in the purification procedure were carried out at 4 °C. In a typical purification, 45 g of frozen cell mass was thawed and resuspended in 225 mL of buffer A [50 mM Tris-chloride (pH 7.6) and 10% (v/v) glycerol] containing 250 μM phenylmethanesulfonyl fluoride (PMSF) and 1 mM 1,10-phenanthroline. The cells were lysed by passage through a French pressure cell at 16 000 psi. Additional 250 μM PMSF was added to the crude cell lysate. After centrifugation at 20000*g* for 10 min to pellet cell debris, 0.2 equiv volumes of 6% (w/v) streptomycin sulfate dissolved in buffer A was dripped into the supernatant with stirring. The resulting suspension was again centrifuged as described above, and the supernatant was brought to 35% of saturation in ammonium sulfate by slow addition of the solid with stirring. This suspension was centrifuged as described above, and the supernatant was brought to 60% of saturation in ammonium sulfate as described above. This suspension was centrifuged, and the pellet (∼ 40 g) was dissolved in 45 mL of buffer A containing 250 μM PMSF and 1 mM 1,10-phenanthroline. The protein solution was dialyzed for ∼8 h in 4 L of buffer A. The resulting ∼90 mL of solution was centrifuged and diluted with an equal volume of buffer A containing 250 μM PMSF. This solution was loaded onto a 600 mL DEAE-Sepharose FF column (Pharmacia) in buffer A. The column was washed with 300 mL of buffer A and then developed with a 1.8 L linear gradient from 0 to 0.4 M NaCl in buffer A. Fractions containing MIOX (subunit molecular mass of 33 kDa) were identified by denaturing polyacrylamide gel electrophoresis (SDS−PAGE) and were combined. The volume of the pool was reduced to <10 mL in an Amicon Diaflow stirred pneumatic concentrator with a YM-10 membrane. Half of the concentrated MIOX solution was loaded onto a 500 mL Sephacryl S-200 HR (Pharmacia) column in buffer A. After elution at 1 mL/min with buffer A, three major peaks that all contained MIOX [as determined by SDS−PAGE and activity assay, which is described in detail in the accompanying paper (*13*)] were observed. The latest-eluting fractions, which had the highest specific activity, were combined and brought to 2−3 mM in MIOX in a Centriprep (Millipore) concentrator with a YM-10 membrane. The purified MIOX was exchanged into buffer C [50 mM Bis-Tris·acetate (pH 6) and 10% (w/w) glycerol] by repeated dilution and volume reduction in the Centriprep concentrator. The progress of buffer exchange was monitored by pH. The concentration of the iron-free MIOX was determined by the absorbance at 280 nm by using the molar absorptivity ($\epsilon_{280} = 60\,800\ M^{-1}\ cm^{-1}$) calculated according to the method of Gill and von Hippel (*16*). A typical yield was 300 mg of protein from 45 g of wet cell mass. SDS−PAGE analysis with Coomassie staining was used to estimate that the protein was >95% pure.

Preparation of Stable Complexes. Procedures to remove O_2 from the protein and buffer C have been described (*15*). Preparation of the different oxidation states (II/II, II/III, and III/III) of the enzyme and their substrate complexes was

carried out in an MBraun anoxic chamber by addition of $Fe(II)_{aq}$ [the ammonium sulfate salt for natural-abundance Fe(II) and the sulfate salt prepared by dissolution of Fe^0 in H_2SO_4 for $^{57}Fe(II)$] to anoxic solutions of the iron-free MIOX protein and appropriate treatment (e.g., with MI, H_2O_2, O_2, or one of these oxidants followed by MI) of the resulting solution. Details of the sample preparations are given in the figure legends.

EPR and Mössbauer Spectroscopy. The spectrometers have been described previously (*14*). Specific conditions are given in the appropriate figure legend. Simulation of Mössbauer spectra was carried out using WMOSS (WEB Research, Edina, MN). Some of the simulations are based on the spin Hamiltonian formalism, given by the following equation, in which the first term describes the electron Zeeman effect, the second term represents the interaction between the electric field gradient and the nuclear quadrupole moment, the third term describes the magnetic hyperfine interactions of the electronic spin with the ^{57}Fe nuclei, and the last term represents the nuclear Zeeman interaction.

$$H = \beta \mathbf{S}\cdot\mathbf{g}\cdot\mathbf{B} + \sum_{i=1}^{2} \frac{\mathbf{eQV}_{zz,i}}{4}\left[I_{z,i}^{\,2} - \frac{I_i(I_i+1)}{3} + \frac{\eta}{3}(I_{x,i}^{\,2} - I_{y,i}^{\,2})\right] + \sum_{i=1}^{2} \mathbf{S}\cdot\mathbf{A}_i\cdot\mathbf{I}_i - \sum_{i=1}^{2} g_n\beta_n\mathbf{B}\cdot\mathbf{I}_i$$

Simulations were carried out with respect to the electronic spin of the ground state ($S = {}^1/_2$) with g values known from EPR. The hyperfine tensors with respect to the total spin, **A**, are related to the intrinsic hyperfine tensors, **a**, by the following relation: $\mathbf{A}_i = c_i\cdot\mathbf{a}_i$, where $c_1 = {}^7/_3$ for the Fe(III) site ($S_1 = {}^5/_2$) and $c_2 = -{}^4/_3$ for the Fe(II) site ($S_2 = 2$).

RESULTS

Preparation and Spectroscopic Characterization of the Diiron(III/III) Form of MIOX and Its Substrate Complex. The 4.2 K/40 mT Mössbauer spectra of samples prepared by mixing iron-free MIOX with 1.2−2.0 equiv of Fe(II) in the absence of O_2 exhibit a single quadrupole doublet. Its parameters (isomer shift, δ, of 1.31 mm/s, quadrupole splitting parameter, ΔE_Q, of 3.24 mm/s, and width, Γ, of 0.6 mm/s) are typical of high-spin Fe(II) ions with nitrogen and oxygen (N/O) ligands (Figure 1A). Addition of *myo*-inositol (MI) does not significantly perturb the Mössbauer spectrum (data not shown). The Mössbauer data do not establish the formation of a diiron(II/II) cluster in MIOX. In general, the spectra of diiron(II/II) complexes are insufficiently distinct from those of mononuclear Fe(II) species for dinuclear coordination to be established by Mössbauer. However, given the evidence presented below for formation of diiron(III/III) and diiron(II/III) states of the protein from such samples, we deem it very likely that a d iiron(II/II) complex does form and hereafter denote this state as MIOX(II/II). The observation that such samples exhibit a low-field ($g \sim 16$), very broad EPR resonance that decays upon conversion to MIOX(II/III) or MIOX(III/III) (Figure S1 of the Supporting Information) is consistent with this conclusion and designation.[2]

The 4.2 K/40 mT Mössbauer spectrum of MIOX(II/II) treated with an excess of either H_2O_2 or O_2 is a broad quadrupole doublet (Figure 1B), which can be simulated with parameters ($\delta = 0.49$ mm/s, $\Delta E_Q = 1.01$ mm/s, and $\Gamma = 0.44$ mm/s) characteristic of N/O-coordinated high-spin Fe(III) species (solid line in Figure 1B) (*18*). The spectrum of this sample recorded in a parallel 6 T magnetic field (Figure 1E) reveals that the Fe(III) site has a diamagnetic ($S = 0$) ground state. This result is consistent with the presence of a diiron(III/III) cluster, in which antiferromagnetic (AF) coupling between the adjacent high-spin Fe(III) ions ($S = {}^5/_2$) gives rise to the experimentally observed $S = 0$ ground state. This form of the protein is termed MIOX(III/III).

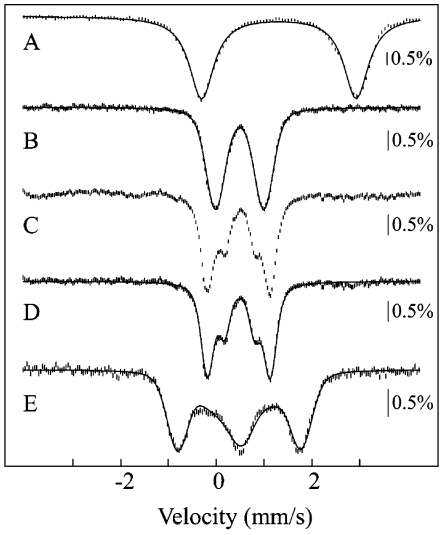

FIGURE 1: 4.2 K Mössbauer spectra of different oxidation states of MIOX. (A) MIOX (0.80 mM) and Fe(II) (1.6 mM). (B and E) MIOX (0.74 mM) and Fe(II) (0.88 mM) after reaction for several minutes at 5 °C with 1.8 equiv of O_2 (added from O_2-saturated buffer). (C) The same solution after addition of MI to a final concentration of 50 mM and incubation for several minutes. A magnetic field of either 40 mT (A−C) or 6 T (E) was applied parallel to the γ-beam. (D) Spectrum C after removal of the contribution of MIOX(II/III)·MI. The solid lines are spectral simulations according to the parameters quoted in the text. In addition, for the spin-Hamiltonian simulation in panel E, an asymmetry parameter η of 0.8 was used, and ΔE_Q was assumed to be positive.

Addition of 50 mM MI perturbs the 4.2 K/40 mT Mössbauer spectrum, eliciting partially resolved quadrupole-doublet components (Figure 1C). Removal of the features of a minor fraction of MIOX(II/III)·MI complex contaminating this sample (see below for characterization of this state) results in the spectrum in Figure 1D, which was analyzed with two quadrupole doublets with the following parameters: $\delta(1) = 0.47$ mm/s, $\Delta E_Q(1) = 1.32$ mm/s, $\Gamma = 0.30$ mm/s, and 69% of total intensity and $\delta(2) = 0.49$ mm/s, $\Delta E_Q(2) = 0.63$ mm/s, $\Gamma = 0.25$ mm/s, and 31% of total intensity. As for the substrate-free form, these Mössbauer parameters are typical of high-spin Fe(III) species and indicate that the substrate binds to or near the cluster, perturbing its spectroscopic properties without changing its oxidation state. For a homogeneous diiron(III/III) cluster, a

[2] If this $g \sim 16$ EPR signal does, as we tentatively conclude, arise form the integer-spin ground state of the MIOX(II/II) complex, then its intensity should increase severalfold when the spectrum is acquired in parallel mode (*17*). We defer presentation and further discussion of the signal until we have tested this prediction.

single quadrupole doublet (for indistinguishable sites) or two doublets with a 1:1 intensity ratio (for resolved sites) would be expected. The experimentally observed 70:30 ratio therefore suggests either that MIOX(III/III) is not saturated at this concentration of MI or that the sample is heterogeneous. To differentiate between these cases, the spectrum was analyzed as the sum of three quadrupole doublet components, of which the first represents MI-free MIOX(III/III) with parameters determined from the spectrum in Figure 1B. The other two quadrupole doublets, which were constrained to have the same intensity, represent the two distinct Fe sites of MI-bound MIOX(III/III). This analysis did not yield satisfactory fits, suggesting that the 70:30 ratio is at least in part due to the presence of multiple MIOX(III/III)·MI complexes with slightly different parameters.

Formation of and Substrate Binding to Mixed-Valent MIOX. More controlled oxidation of MIOX(II/II) with O_2, either by mixing with a solution that delivers a *limiting* quantity (e.g., 0.5 O_2/MIOX ratio) or by slow diffusion of the gas into a MIOX(II/II) solution containing ascorbate or L-cysteine [this procedure, which we term the "O_2-diffusion method", is described in detail in the accompanying paper (*13*)], produces a distinct oxidized form of the protein. Mössbauer and EPR spectra of samples prepared according to this method demonstrate the formation of an AF-coupled, valence-localized, high-spin diiron(II/III) cluster with an $S = {}^1/_2$ ground state, which is perturbed upon binding of MI. These forms are denoted MIOX(II/III) and MIOX(II/III)·MI, respectively.

EPR Spectroscopic Characterization of MIOX(II/III) and MIOX(II/III)·MI. MIOX(II/III) exhibits a very broad, axial EPR signal (Figure 2A, top spectrum), which has effective *g* values of ~1.95, ~1.66, and ~1.66 and is readily detected only at relatively low temperatures and high microwave powers (compare middle spectra in Figure 2A,B). The additional sharper features seen in Figure 2A (marked with an asterisk) and more clearly at higher temperatures and lower powers (Figure 2B) make up a sextet signal typical of ^{55}Mn(II). This signal is present in samples of the iron-free MIOX and can be removed by subtraction of the spectra of a control sample (middle and bottom spectra in Figure 2A,B). The substoichiometric quantity of Mn(II) that it represents is most likely a contaminant.[3] Addition of 3 mM MI to a sample of MIOX(II/III) results in significant changes to the EPR spectrum (bottom spectra in Figure 2A,B). The signal of MIOX(II/III)·MI is axial, is narrower than that of MIOX(II/III), and has effective *g* values of ~1.95, ~1.81, and ~1.81. Moreover, it is readily observed at higher temperatures and lower microwave powers (e.g., 20 K and 0.10 mW). The signals attributed to MIOX(II/III) and

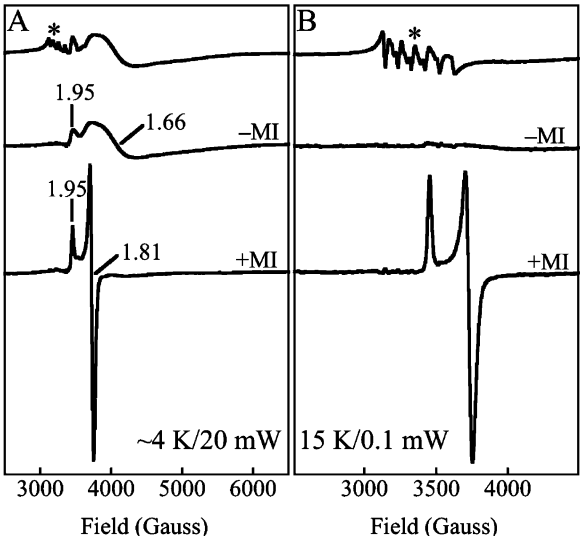

FIGURE 2: X-Band EPR spectra (A) at ~4 K (nominal temperature indicated by the Oxford cryostat) and 20 mW and (B) at 15 K and 0.10 mW of samples containing MIOX(II/III) and MIOX(II/III)·MI. A solution of 0.94 mM MIOX, 1.9 mM Fe(II), and 4 mM sodium ascorbate was subjected to the O_2 diffusion treatment described in the accompanying paper (*13*). The top and middle spectra are for the sample after this treatment. The bottom spectra are for the sample after addition of MI to the O_2-treated solution to 50 mM. To prepare the top spectra in both panels A and B, the spectra of a blank sample containing only the buffer were subtracted from the spectra of the MI-free sample to remove a $g = 2.00$ signal that is intrinsic to the EPR cavity. To prepare the middle spectra, the spectra of a control sample lacking MIOX(II/III) were subtracted from the experimental spectra to remove both the $g = 2.00$ signal and the six-line signal attributed to contaminating Mn(II). To prepare the bottom spectra, the spectra of the control sample were subtracted from those of the MIOX(II/III)·MI sample to remove the $g = 2.00$ and Mn(II) signals. Integration of the bottom spectrum in B and comparison to the spectrum of a standard gave a MIOX(II/III)·MI contration of 0.56 mM (0.6 equiv relative to total MIOX). Spectral parameters: microwave frequency, 9.45 GHz; modulation amplitude, 10 G; modulation frequency, 100 kHz; receiver gain, 1.25×10^4; time constant, 327 ms; sweep width, 8000 (A) and 2000 G (B); points per spectrum, 2048 (A) and 1024 (B); scan time, 336 (A) and 168 s (B).

MIOX(II/III)·MI are typical of AF-coupled, high-spin diiron(II/III) clusters. These clusters exhibit $S = {}^1/_2$ EPR signals with a $g_{average}$ of <2. Quantum-mechanical mixing of excited spin states with the $S = {}^1/_2$ ground state increases the anisotropy of **g**, as has been described in detail in the literature (*19*, *20*). The extent of this mixing depends on the zero-field splitting parameters and the energy separations between the ground and excited spin states; it increases with a decreasing strength of the exchange coupling interaction (*19*, *20*). For example, hydroxo-bridged, high-spin diiron(II/III) clusters exhibit significantly greater **g**-anisotropy and weaker exchange coupling compared to the corresponding oxo-bridged compounds (*21*). Consequently, the diminished spread of the effective *g*-values for MIOX(II/III)·MI compared to those for MIOX(II/III) demonstrates a significant perturbation of the electronic structure, probably involving a strengthening of the exchange coupling between the Fe(II) and Fe(III) sites, upon binding of MI. Furthermore, the extreme breadth of the EPR signal of MIOX(II/III) indicates the presence of **g** strain, which most likely reflects the presence of different cluster conformations with

[3] The sextet signal is indicative of the presence of a Mn(II) species with a half-integer-spin ground state. The six lines arise from hyperfine coupling to a single ^{55}Mn nucleus: a greater number of hyperfine interactions would be expected for a dinuclear species [e.g., a dimanganese(II/III) or -(III/IV) cluster]. The putative Mn(II) species copurifies with iron-free MIOX and amounts to 0.25−0.5 equiv. Unlike the spectra of the diiron MIOX complexes, the EPR spectrum attributed to Mn(II) is unaffected by addition of MI or DG, and its intensity does not vary with reaction time during turnover (*13*). The purified MIOX is inactive in the absence of Fe(II), even in the presence of additional Mn(II). Moreover, inclusion of Mn(II) in the assay at a concentration equal to that of Fe(II) (at either ≤1 or >1000 equiv of each relative to MIOX) has no effect on activity. We therefore tentatively conclude that the Mn(II) is a contaminant, but a structural or catalytic role distinct from that of the diiron cluster cannot yet be ruled out.

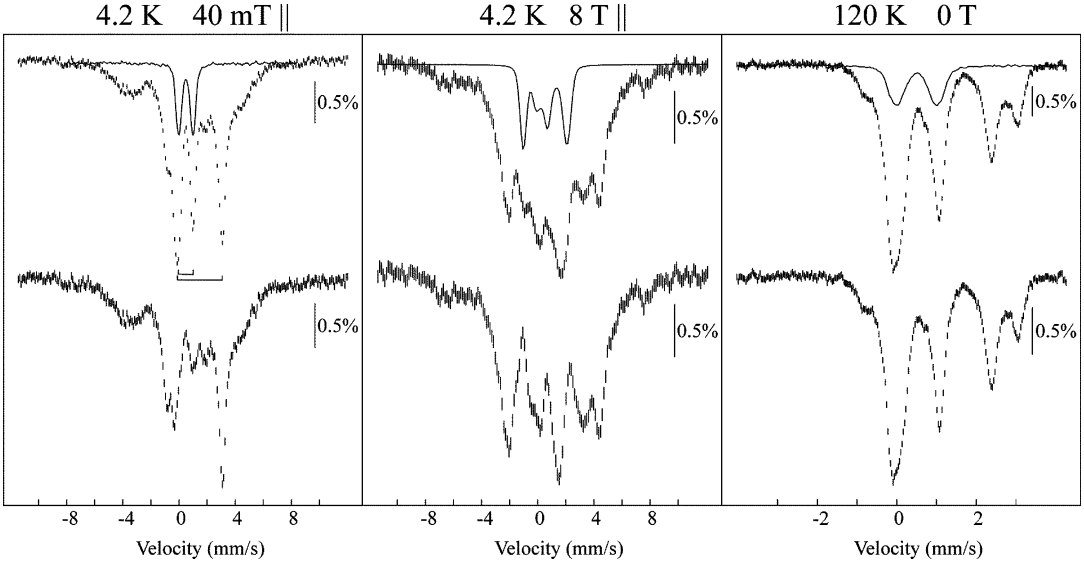

FIGURE 3: Mössbauer spectra of MIOX(II/III). A sample of 1.0 mM MIOX and 2.0 mM ^{57}Fe(II) was reacted at 5 °C for several minutes with 0.5 equiv of O_2 (delivered from O_2-saturated buffer). Experimental conditions are given above the spectra. The top spectra show raw data (hashed marks) and the contribution of MIOX(III/III) (15% of the total intensity, solid line). Spectra of MIOX(II/III) were obtained by removing the 5 and 15% contributions from MIOX(II/II) and MIOX(III/III), respectively, and are shown at the bottom of each panel.

different ratios of J and $D_{Fe(II)}$ values, as observed for sMMO (*20*).

Mössbauer Spectroscopic Characterization of MIOX(II/III) and MIOX(II/III)·MI. The 4.2 K/40 mT Mössbauer spectrum of a sample prepared by treating MIOX(II/II) with 0.5 equiv of O_2 (Figure 3, top left) exhibits poorly resolved broad features, in addition to quadrupole doublets from MIOX(III/III) and unreacted MIOX(II/II) (indicated with brackets). At 120 K in the absence of a magnetic field, the paramagnetic features collapse to quadrupole doublets with parameters typical of high-spin Fe(III) and Fe(II) sites (Figure 3, top right) (*18*).[4] Analysis of this spectrum reveals that this particular sample contained 45 ± 5% high-spin Fe(II) and 55 ± 5% high-spin Fe(III) sites. From the spectrum of the same sample recorded in a strong (8 T) applied field (Figure 3, top middle), the maximum contribution from MIOX(III/III) can be set as 15% of the total intensity, because its features can be easily simulated due to its $S = 0$ ground state (see above). The quantity of Fe(II) not in the form of MIOX(II/III) is less easily assessed, because it does not have well-resolved features in the high-field spectrum. In the low or zero field, its quadrupole doublet overlaps either with the Fe(II) quadrupole doublet(s) from MIOX(II/III) (120 K/zero field) or with the broad, magnetically split features of MIOX(II/III) (4.2 K/40 mT). From the total quantity of Fe(II) and Fe(III) deduced from the 120 K/zero field spectrum, it is clear that only a small quantity (approximately 5% of the Fe) should be Fe(II) that is not associated with MIOX(II/III). Removal of the contributions of MIOX(III/III) (15%) and MIOX(II/II) (5%) yields reference spectra for MIOX(II/III) (Figure 3, bottom). The 120 K/zero field spectrum suggests that this state is conformationally heterogeneous. The 4.2 K spectra of MIOX(II/III) show mostly broad features. To evaluate the possibility that the breadth of the spectra is caused by a fluctuation rate of the electronic spin that is comparable to the ^{57}Fe Larmor frequency, the 40 mT spectrum was recorded at 2 K. This spectrum (not shown) is essentially identical to the 4.2 K/40 mT spectrum, suggesting that the broad features are not a consequence of intermediate relaxation. Rather, as noted above in analysis of the EPR spectrum, the breadth is likely to be caused by variation in the values of spin-Hamiltonian parameters [in particular J and $D_{Fe(II)}$] resulting from heterogeneity in the structure or conformation of the diiron cluster in MIOX(II/III).

In stark contrast to the poorly resolved features of MIOX(II/III), MIOX(II/III)·MI yields well-resolved Mössbauer features. Detailed Mössbauer spectroscopic analysis of MIOX(II/III)·MI was carried out on a sample containing a saturating concentration (100 mM) of MI; this sample was prepared by the O_2 diffusion method described in detail in the accompanying paper (*13*). Of all procedures thus far tested, this method gives the highest and most consistent yield of the mixed-valent complex. Analysis of six spectra recorded under different experimental conditions reveals that the sample contains 34 ± 3% MIOX(II/II) (presumably with MI bound), 5 ± 3% MIOX(III/III)·(MI), and 61 ± 5% MIOX(II/III)·MI. Removal of the contribution of MIOX(II/II)·(MI) and MIOX(III/III)·(MI) yields reference spectra of MIOX(II/III)·MI.[5] The 120 K/zero field spectrum

[4] Approximate Mössbauer parameters of the Fe(II) and Fe(III) components are as follows: $\delta(1) \approx 1.2$ mm/s, $\Delta E_Q(1) \approx 3.3$ mm/s, $\delta(2) \approx 1.2$ mm/s, and $\Delta E_Q(2) \approx 3.3$ mm/s for the Fe(II) sites and $\delta \approx 0.5$ mm/s and $\Delta E_Q \approx 1.0$ mm/s for the Fe(III) site. In addition, the 120 K/zero field spectra of samples containing MIOX(II/III) or MIOX(II/III)·MI exhibit a weak shoulder at −1 mm/s that is currently not well-understood. This feature amounts to approximately 3% of the total intensity. Its shape and intensity do not vary in the temperature range of 100−150 K, suggesting that it does not arise from a paramagnetic species with intermediate relaxation. The nature of the associated species is not known, but it represents only a minor fraction of the sample.

[5] Experimental spectra of MIOX(II/II) were used for the subtraction analysis. For MIOX(III/III) in the presence of substrate, experimental spectra were used for the 4.2 K/40 mT and 120 K/zero field spectra. For spectra recorded at 4.2 K in large external fields, a simulation based on the parameters obtained from the 4.2 K/40 mT spectrum, an asymmetry parameter, η, of 0.8, and the assumption of diamagnetism was used.

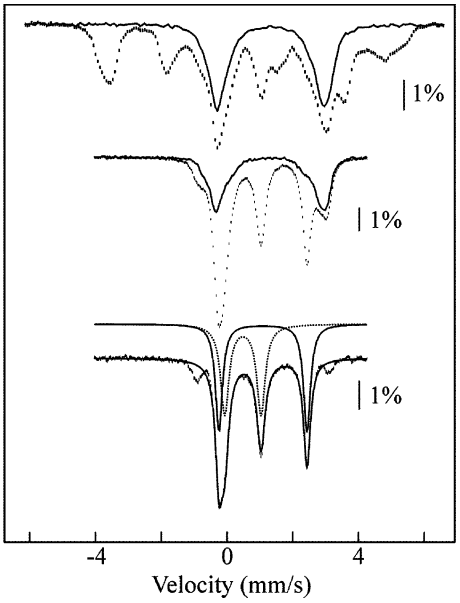

FIGURE 4: Mössbauer spectra (4.2 K/40 mT, top; 120 K/zero field, middle) of a sample subjected to the O_2 diffusion treatment described in the accompanying paper (*13*) and then treated with 100 mM MI. Removal of the 34 and 5% contribution of MIOX(II/II)·(MI) and MIOX(III/III)·MI from the 120 K/zero field spectrum yields the 120 K/zero field spectrum of MIOX(II/III)·MI (bottom). The solid line overlaid with the data is a simulation according to the parameters from fit 1 in the text, and the solid and dotted lines plotted above the data are the contributions of the Fe(II) and Fe(III) sites, respectively.

of MIOX(II/III)·MI (Figure 4, bottom) can be analyzed as the superposition of two quadrupole doublets with parameters typical of high-spin Fe(II) and Fe(III) ions. Two fits, which are similar in quality but different in the configuration of the four lines (nested vs alternating), are obtained. For fit 1, $\delta(1) = 0.48$ mm/s, $\Delta E_Q(1) = 1.10$ mm/s, $\delta(2) = 1.09$ mm/s, and $\Delta E_Q(2) = 2.68$ mm/s. For fit 2, $\delta(1) = 0.39$ mm/s, $\Delta E_Q(1) = 1.28$ mm/s, $\delta(2) = 1.18$ mm/s, and $\Delta E_Q(2) = 2.51$ mm/s. The 4.2 K reference spectra of MIOX(II/III)·MI recorded in parallel magnetic fields of 40 mT and 3, 6, and 8 T exhibit several sharp peaks ranging from −4 to 5 mm/s. As the intensities of the six lines of magnetic Mössbauer spectra of species with an $S = {}^1/_2$ ground state depend on the orientation of the magnetic field relative to the γ-beam, the 4.2 K spectrum of this sample in a perpendicular 40 mT magnetic field was also measured. The 4.2 K spectra of MIOX(II/III)·MI derived from the subtraction analysis (Figure 5) are typical of a valence-localized, high-spin diiron(II/III) cluster in the slow relaxation limit and can be simulated according to the spin-Hamiltonian formalism (see Materials and Methods). The parameters used (Table 1) in the simulations (Figure 3) are similar to those observed for other valence-localized high-spin diiron(II/III) clusters (*20*, *22*). The values of δ and ΔE_Q used for this analysis are those from fit 1 to the 120 K/zero field spectrum, with isomer shifts corrected by 0.03 mm/s for the second-order Doppler shift; these values were fixed during fitting of the field-dependent, 4.2 K spectra. When δ and ΔE_Q were allowed to vary, their values changed by less than ±0.03 mm/s. The Mössbauer parameters from fit 2 to the 120 K/zero field spectrum were also tested in spin-Hamiltonian simulations of the field-dependent 4.2 K spectra. In general, these simulated spectra agreed less well with the experimental spectra. In particular, the lines of the Fe(II) site in the 40 mT spectrum are fit better with the lower isomer shift of fit 1.

Table 1: Mössbauer Parameters of MIOX(II/III)·MI

	δ (mm/s)	ΔE_Q (mm/s)[a]	η[a]	$A/g_N\beta_N$ (T)[a]
Fe(III) site	0.49	−1.11	7.2	(−43.1, −55.8, −53.4)
Fe(II) site	1.12	2.68	0.3	(26.5, 22.5, 11.6)

[a] The simulation was carried out with respect to the total spin ($S = {}^1/_2$) with $g = 1.95$, 1.81, and 1.81; all tensors were assumed to be collinear.

DISCUSSION

The spectroscopic data demonstrate the presence in MIOX of a non-heme, dinuclear iron cluster that is stable in its II/III and III/III oxidation states (and presumably also its II/II state) and that is significantly perturbed upon binding of the substrate, *myo*-inositol (MI). Thus, MIOX is a new member of the non-heme diiron protein family, which also includes the R2 subunit of class I ribonucleotide reductase

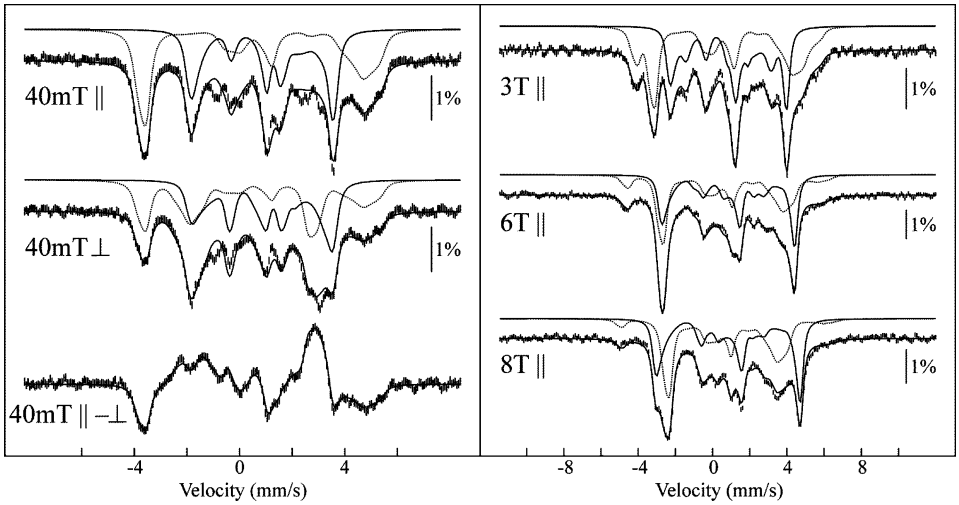

FIGURE 5: 4.2 K Mössbauer spectra of MIOX(II/III)·MI. All spectra were obtained by removal of the contributions of MIOX(II/II)·(MI) (34%, solid line) and MIOX(III/III)·MI (5%) from the spectra of the sample from Figure 4. The externally applied field is indicated below each spectrum. The solid lines overlaid with the data are spin-Hamiltonian simulations according to parameters reported in Table 1, and the solid and dotted lines above the data are the contributions of the Fe(II) and Fe(III) sites, respectively.

(RNR-R2), soluble methane monooxygenase (sMMO), toluene monooxygenases, alkane ω-hydroxylase, stearoyl acyl carrier protein Δ^9-desaturase, ferritin, hemerythrin, and purple acid phosphatases (*23*−*27*). Members of the oxygenase/oxidase subset of this family use their diiron clusters to effect two-electron or one-electron oxidation reactions (hydroxylation or desaturation of an exogenous substrate or oxidation of an endogenous tyrosine residue to a tyrosyl radical in RNR-R2) (*25*, *28*−*31*). The reaction catalyzed by MIOX, a C−C-bond-cleaving, four-electron oxidation of MI to DG (*1*, *2*), thus expands the known collective chemical capabilities of the non-heme diiron oxygenase/oxidase subfamily.

Many of the aforementioned non-heme diiron proteins have structurally similar four-helix bundles (*24*, *32*). Conserved EXXH motifs within two of the four helices contribute a total of four ligands to the diiron cluster. Known MIOX sequences lack even a single conserved copy of this motif. An alignment of the rat, mouse, human, and pig sequences revealed a single conserved *D*XXH motif (*11*), but inclusion of probable MIOX sequences from more distantly related organisms (e.g., *Xenopus tropicalis*) in alignments shows that this motif is not conserved (not shown). In general, the primary structure of MIOX fails to provide obvious clues about its tertiary structure or the nature of its diiron site: similarity searches of databases with the mouse MIOX sequence as query yield a very high degree of similarity (>45%) to confirmed or probable MIOX orthologues but insignificant global similarity to any protein that has been structurally characterized. Given the chemical novelty and physiological importance of the MIOX reaction, structural characterization of the protein is clearly warranted.

Oxidation of MIOX(II/II) by excess O_2 or H_2O_2 results in generation of an AF-coupled, high-spin diiron(III/III) cluster, producing MIOX(III/III). Addition of substrate, MI, perturbs the Mössbauer features, but the resulting substrate-bound diiron(III/III) state appears to be heterogeneous. Oxidation of MIOX(II/II) by a limiting quantity of O_2 or in the presence of reductants results in accumulation of the mixed-valent form of the protein, MIOX(II/III). The EPR and Mössbauer spectra of this form show that the Fe ions of the cluster are high-spin and AF-coupled and that the cluster is valence-localized. The broad spectra are suggestive of weak exchange coupling between the Fe(III) and Fe(II) sites and, again, the presence of different cluster conformations with different spin-Hamiltonian parameters. Binding of MI strongly perturbs the spectroscopic properties of the cluster and produces a complex, MIOX(II/III)·MI, that appears to be more homogeneous. Data in the accompanying paper (*13*) show that it is this complex that activates O_2 for DG production.

Qualitatively, the spectral perturbations associated with binding of MI to MIOX(II/III) are strikingly reminiscent of, albeit opposite to, those caused by binding of phosphate to the diiron(II/III) form of the phosphoprotein phosphatase, uteroferrin (Uf). Like MIOX(II/III)·MI, Uf(II/III) exhibits sharp Mössbauer (*22*, *33*) and EPR spectra (*34*, *35*), and the latter signal is readily detected at higher temperatures (e.g., 20 K) and moderate microwave powers. Conversely, Uf(II/III)·phosphate, like MIOX(II/III), exhibits broader spectra (*22*, *36*, *37*), and the EPR signal is readily detected only at lower temperatures (e.g., 8 K) and high powers (*37*). Binding of phosphate to Uf(II/III) weakens the exchange coupling from 20 to 6 cm^{-1} ($H = J\mathbf{S}_1\cdot\mathbf{S}_2$) (*37*, *38*). Thus, the correlation of spectroscopic properties suggests that MI binding may *strengthen* exchange coupling between the Fe(II) and Fe(III) ions in mixed-valent MIOX.

Two mechanisms for the effect may be envisaged. The first would involve induction of a protein conformational change, involving residues near or directly coordinating the diiron cluster, by binding of MI in the vicinity of, but not directly to, the cluster. There are at least two precedents for this mechanism. First, it was shown that binding of protein B of sMMO to the diiron(II/III) form of the hydroxylase component results in a decrease in J from 60 to 10 cm^{-1} (*20*). This effect almost certainly results indirectly from a conformational change rather than directly by interaction of protein B with the diiron(II/III) cluster. Second, it has been shown for several mononuclear Fe(II) oxygenases that binding of the substrate causes dissociation of a water ligand and creates an open coordination site, which is believed to be the site to which O_2 adds to initiate the reaction (*28*). In some cases, the activating coordination change is accompanied by a reduction in the Mössbauer isomer shift (*14*, *39*). Analysis of the field-dependent, 4.2 K Mössbauer spectra of MIOX(II/III)·MI favors a rather low isomer shift for the Fe(II) site (1.12 mm/s). If δ for the Fe(II) site in MIOX(II/III) should prove to be larger, it would be consistent with the notion that MI binding induces a similar activating change in the coordination of the Fe(II) site of mixed-valent MIOX. Rigorous evaluation of this hypothesis will require definitive assignment of the isomer shifts of the Fe(II) sites in MIOX(II/III) and MIOX(II/III)·MI. This assignment would be facilitated by selective enrichment of only one of the two Fe sites of the diiron cluster with the Mössbauer-active isotope, ^{57}Fe, which may be achievable if the two Fe sites have different affinities (*40*).

The second possible origin of the effect of MI binding, which we favor on the basis of mechanistic considerations discussed below and more fully in the accompanying paper (*13*), would involve binding of MI directly to the diiron(II/III) cluster in MIOX. This is the mechanism by which binding of phosphate to Uf(II/III) exerts its effects: the crystal structure of the Uf·phosphate complex reveals direct μ-1,3-phosphate coordination (*41*). The presence of the phosphate bridge somehow reduces the strength of the AF exchange coupling. The simplest possibility for the opposite effect of the binding event in MIOX is that an alkoxide bridge from MI provides a more efficient pathway for superexchange than any bridging ligands that may be present in substrate-free MIOX(II/III), thereby *increasing* the strength of the AF coupling. Values of J of ~20 cm^{-1} have been reported for hydroxo- and phenoxo-bridged, valence-localized, high-spin diiron(II/III) species (*42*, *43*), similar to the J reported for Uf(II/III). Thus, coordination of a μ-alkoxide bridge from MI between the Fe ions could give a J of the magnitude expected on the basis of the analogy to Uf(II/III). Binding to effect ionization of the C1 hydroxyl group could direct the C1-bonded hydrogen toward the open site on the Fe(II) to which O_2 adds to undergo activation. The resulting reactive intermediate could then cleave the C1−H bond, with facilitation by the Fe-coordinated oxyanion, to initiate turnover. Regardless of the details of subsequent processing to D-glucuronate, the mechanism of substrate and O_2 activation would be novel for a diiron oxygenase.

ACKNOWLEDGMENT

We thank Professor Edward I. Solomon for helpful discussion of the literature on uteroferrin and the reviewers for their helpful suggestions.

SUPPORTING INFORMATION AVAILABLE

X-band EPR spectra at ~4 K in the low-field region of samples of MIOX(II/II) and MIOX(II/III). This material is available free of charge via the Internet at http://pubs.acs.org.

REFERENCES

1. Charalampous, F. C., and Lyras, C. (1957) Biochemical studies on inositol. IV. Conversion of inositol to glucuronic acid by rat kidney extracts, *J. Biol. Chem. 228*, 1−13.
2. Charalampous, F. C. (1959) Biochemical studies on inositol. V. Purification and properties of the enzyme that cleaves inositol to D-glucuronic acid, *J. Biol. Chem. 234*, 220−227.
3. Moskala, R., Reddy, C. C., Minard, R. D., and Hamilton, G. A. (1981) An oxygen-18 tracer investigation of the mechanism of *myo*-inositol oxygenase, *Biochem. Biophys. Res. Commun. 99*, 107−113.
4. Hankes, L. V., Politzer, W. M., Touster, O., and Anderson, L. (1969) *myo*-Inositol catabolism in human pentosurics: The predominant role of the glucuronate-xylulose-pentose phosphate pathway, *Ann. N.Y. Acad. Sci. 165*, 564−576.
5. Stribling, D., Armstrong, F. M., and Harrison, H. E. (1989) Aldose reductase in the etiology of diabetic complications: 2. Nephropathy, *Journal of Diabetic Complications 3*, 70−76.
6. Cohen, A. M., Wald, H., Popovtzer, M., and Rosenmann, E. (1995) Effect of *myo*-inositol supplementation on the development of renal pathological changes in the Cohen diabetic (type 2) rat, *Diabetologia 38*, 899−905.
7. Crabbe, M. J., and Goode, D. (1998) Aldose reductase: A window to the treatment of diabetic complications? *Prog. Retinal Eye Res. 17*, 313−383.
8. Khandelwal, M., Reece, E. A., Wu, Y. K., and Borenstein, M. (1998) Dietary *myo*-inositol therapy in hyperglycemia-induced embryopathy, *Teratology 57*, 79−84.
9. Sundkvist, G., Dahlin, L. B., Nilsson, H., Eriksson, K. F., Lindgarde, F., Rosen, I., Lattimer, S. A., Sima, A. A., Sullivan, K., and Greene, D. A. (2000) Sorbitol and *myo*-inositol levels and morphology of sural nerve in relation to peripheral nerve function and clinical neuropathy in men with diabetic, impaired, and normal glucose tolerance, *Diabetes Med. 17*, 259−268.
10. Prabhu, K. S., Arner, R. J., Vunta, H., and Reddy, C. C. (2005) Up-regulation of human *myo*-inositol oxygenase by hyperosmotic stress in renal proximal tubular epithelial cells, *J. Biol. Chem. 280*, 19895−19901.
11. Arner, R. J., Prabhu, K. S., Thompson, J. T., Hildenbrandt, G. R., Liken, A. D., and Reddy, C. C. (2001) *myo*-Inositol oxygenase: Molecular cloning and expression of a unique enzyme that oxidizes *myo*-inositol and D-*chiro*-inositol, *Biochem. J. 360*, 313−320.
12. Arner, R. J., Prabhu, K. S., and Reddy, C. C. (2004) Molecular cloning, expression, and characterization of *myo*-inositol oxygenase from mouse, rat, and human kidney, *Biochem. Biophys. Res. Commun. 324*, 1386−1392.
13. Xing, G., Barr, E. W., Diao, Y., Hoffart, L. M., Prabhu, K. S., Arner, R. J., Reddy, C. C., Krebs, C., and Bollinger, J. M., Jr. (2006) Oxygen Activation by a Mixed-Valent, Diiron(II/III) Cluster in the Glycol-Cleavage Reaction Catalyzed by *myo*-Inositol Oxygenase, *Biochemistry 45*, 5402−5412.
14. Price, J. C., Barr, E. W., Tirupati, B., Bollinger, J. M., Jr., and Krebs, C. (2003) The first direct characterization of a high-valent iron intermediate in the reaction of an α-ketoglutarate-dependent dioxygenase: A high-spin Fe(IV) complex in taurine/α-ketoglutarate dioxygenase (TauD) from *Escherichia coli*, *Biochemistry 42*, 7497−7508.
15. Parkin, S. E., Chen, S., Ley, B. A., Mangravite, L., Edmondson, D. E., Huynh, B. H., and Bollinger, J. M., Jr. (1998) Electron Injection through a Specific Pathway Determines the Outcome of Oxygen Activation at the Diiron Cluster in the F208Y Mutant of *Escherichia coli* Ribonucleotide Reductase Protein R2, *Biochemistry 37*, 1124−1130.
16. Gill, S. C., and von Hippel, P. H. (1989) Calculation of Protein Extinction Coefficients from Amino Acid Sequence Data, *Anal. Biochem. 182*, 319−326.
17. Hendrich, M. P., Münck, E., Fox, B. G., and Lipscomb, J. D. (1990) Integer-spin EPR studies of the fully reduced methane monooxygenase hydroxylase component, *J. Am. Chem. Soc. 112*, 5861−5865.
18. Gütlich, P., Link, R., and Trautwein, A. X. (1978) *Mössbauer Spectroscopy and Transition Metal Chemistry*, Springer-Verlag, Berlin.
19. Guigliarelli, B., Bertrand, P., and Gayda, J. P. (1986) Contribution of the fine structure terms to the *g* values of the biological iron(III)-iron(II) clusters, *J. Chem. Phys. 85*, 1689−1692.
20. Fox, B. G., Hendrich, M. P., Surerus, K. K., Andersson, K. K., Froland, W. A., Lipscomb, J. D., and Münck, E. (1993) Mössbauer, EPR, and ENDOR studies of the hydroxylase and reductase components of methane monooxygenase from *Methylosinus trichosporium* OB3b, *J. Am. Chem. Soc. 115*, 3688−3701.
21. Davydov, R., Kuprin, S., Gräslund, A., and Ehrenberg, A. (1994) Electron Paramagnetic Resonance Study of the Mixed-Valent Diiron Center in *Escherichia coli* Ribonucleotide Reductase Produced by Reduction of Radical-Free Protein R2 at 77 K, *J. Am. Chem. Soc. 116*, 11120−11128.
22. Rodriguez, J. H., Ok, H. N., Xia, Y.-M., Debrunner, P. G., Hinrichs, B. E., Meyer, T., and Packard, N. H. (1996) Mössbauer Spectroscopy of the Spin-Coupled Fe^{3+}-Fe^{2+} Center of Reduced Uteroferrin, *J. Phys. Chem. 100*, 6849−6862.
23. Vincent, J. B., Olivier-Lilley, G. L., and Averill, B. A. (1990) Proteins containing oxo-bridged dinuclear iron centers: A bioinorganic perspective, *Chem. Rev. 90*, 1447−1467.
24. Nordlund, P., and Eklund, H. (1995) Di-iron-carboxylate Proteins, *Curr. Opin. Struct. Biol. 5*, 758−766.
25. Wallar, B. J., and Lipscomb, J. D. (1996) Dioxygen activation by enzymes containing binuclear non-heme iron clusters, *Chem. Rev. 96*, 2625−2657.
26. Kurtz, D. M., Jr. (1997) Structural similarity and functional diversity in diiron-oxo proteins, *J. Biol. Inorg. Chem. 2*, 159−167.
27. Tshuva, E. Y., and Lippard, S. J. (2004) Synthetic Models for Non-Heme Carboxylate-Bridged Diiron Metalloproteins: Strategies and Tactics, *Chem. Rev. 104*, 987−1011.
28. Solomon, E. I., Brunold, T. C., Davis, M. I., Kemsley, J. N., Lee, S.-K., Lehnert, N., Neese, F., Skulan, A. J., Yang, Y.-S., and Zhou, J. (2000) Geometric and Electronic Structure/Function Correlations in Non-Heme Iron Enzymes, *Chem. Rev. 100*, 235−349.
29. Merkx, M., Kopp, D. A., Sazinsky, M. H., Blazyk, J. L., Müller, J., and Lippard, S. J. (2001) Dioxygen activation and methane hydroxylation by soluble methane monooxygenase: A tale of two irons and three proteins, *Angew. Chem., Int. Ed. 40*, 2782−2807.
30. Fox, B. G., Lyle, K. S., and Rogge, C. E. (2004) Reactions of the Diiron Enzyme Stearoyl-Acyl Carrier Protein Desaturase, *Acc. Chem. Res. 37*, 421−429.
31. Krebs, C., Price, J. C., Baldwin, J., Saleh, L., Green, M. T., and Bollinger, J. M., Jr. (2005) Rapid Freeze-Quench ^{57}Fe Mössbauer Spectroscopy: Monitoring Changes of an Iron-Containing Active Site during a Biochemical Reaction, *Inorg. Chem. 44*, 742−757.
32. Summa, C. M., Lombardi, A., Lewis, M., and DeGrado, W. F. (1999) Tertiary templates for the design of diiron proteins, *Curr. Opin. Struct. Biol. 9*, 500−508.
33. Debrunner, P. G., Hendrich, M. P., De Jersey, J., Keough, D. T., Sage, J. T., and Zerner, B. (1983) Mössbauer and EPR study of the binuclear iron center in purple acid phosphatase, *Biochim. Biophys. Acta 745*, 103−106.
34. Davis, J. C., and Averill, B. A. (1982) Evidence for a spin-coupled binuclear iron unit at the active site of the purple acid phosphatase from beef spleen, *Proc. Natl. Acad. Sci. U.S.A. 79*, 4623−4627.
35. Antanaitis, B. C., Aisen, P., and Lilienthal, H. R. (1983) Physical characterization of two-iron uteroferrin. Evidence for a spin-coupled binuclear iron cluster, *J. Biol. Chem. 258*, 3166−3172.
36. Pyrz, J. W., Sage, J. T., Debrunner, P. G., and Que, L., Jr. (1986) The interaction of phosphate with uteroferrin. Characterization of a reduced uteroferrin-phosphate complex, *J. Biol. Chem. 261*, 11015−11020.
37. Day, E. P., David, S. S., Peterson, J., Dunham, W. R., Bonvoisin, J. J., Sands, R. H., and Que, L., Jr. (1988) Magnetization and electron paramagnetic resonance studies of reduced uteroferrin and its "EPR-silent" phosphate complex, *J. Biol. Chem. 263*, 15561−15567.

38. Yang, Y.-S., McCormick, J. M., and Solomon, E. I. (1997) Circular dichroism and magnetic circular dichroism studies of the mixed-valence binuclear non-heme iron active site in uteroferrin and its anion complexes, *J. Am. Chem. Soc. 119*, 11832−11842.
39. Wolgel, S. A., Dege, J. E., Perkins-Olson, P. E., Juarez-Garcia, C. H., Crawford, R. L., Münck, E., and Lipscomb, J. D. (1993) Purification and characterization of protocatechuate 2,3-dioxygenase from *Bacillus macerans*: A new extradiol catecholic dioxygenase, *J. Bacteriol. 175*, 4414−4426.
40. Bollinger, J. M., Jr., Chen, S., Parkin, S. E., Mangravite, L. M., Ley, B. A., Edmondson, D. E., and Huynh, B. H. (1997) Differential Iron(II) Affinity of the Sites of the Diiron Cluster in R2 of *Escherichia coli* Ribonucleotide Reductase: Tracking the Individual Sites through the O_2 Activation Sequence, *J. Am. Chem. Soc. 119*, 5976−5977.
41. Guddat, L. W., McAlpine, A. S., Hume, D., Hamilton, S., Jersey, J. d., and Martin, J. L. (1999) Crystal structure of mammalian purple acid phosphatase, *Structure 7*, 757−767.
42. Bossek, U., Hummel, H., Weyhermüller, T., Bill, E., and Wieghardt, K. (1996) The first μ-(OH)-bridged model complex for the mixed-valent $Fe^{II}Fe^{III}$ form of hemerythrin, *Angew. Chem., Int. Ed. 34*, 2642−2645.
43. Mashuta, M. S., Webb, R. J., McCusker, J. K., Schmitt, E. A., Oberhausen, K. J., Richardson, J. F., Buchanan, R. M., and Hendrickson, D. N. (1992) Electron transfer in iron(II)iron(III) model complexes of iron-oxo proteins, *J. Am. Chem. Soc. 114*, 3815−3827.

BI0519607